iScience

CellPress

Article

Optimal Scaling of Critical Size for Metamorphosis in the Genus *Drosophila*

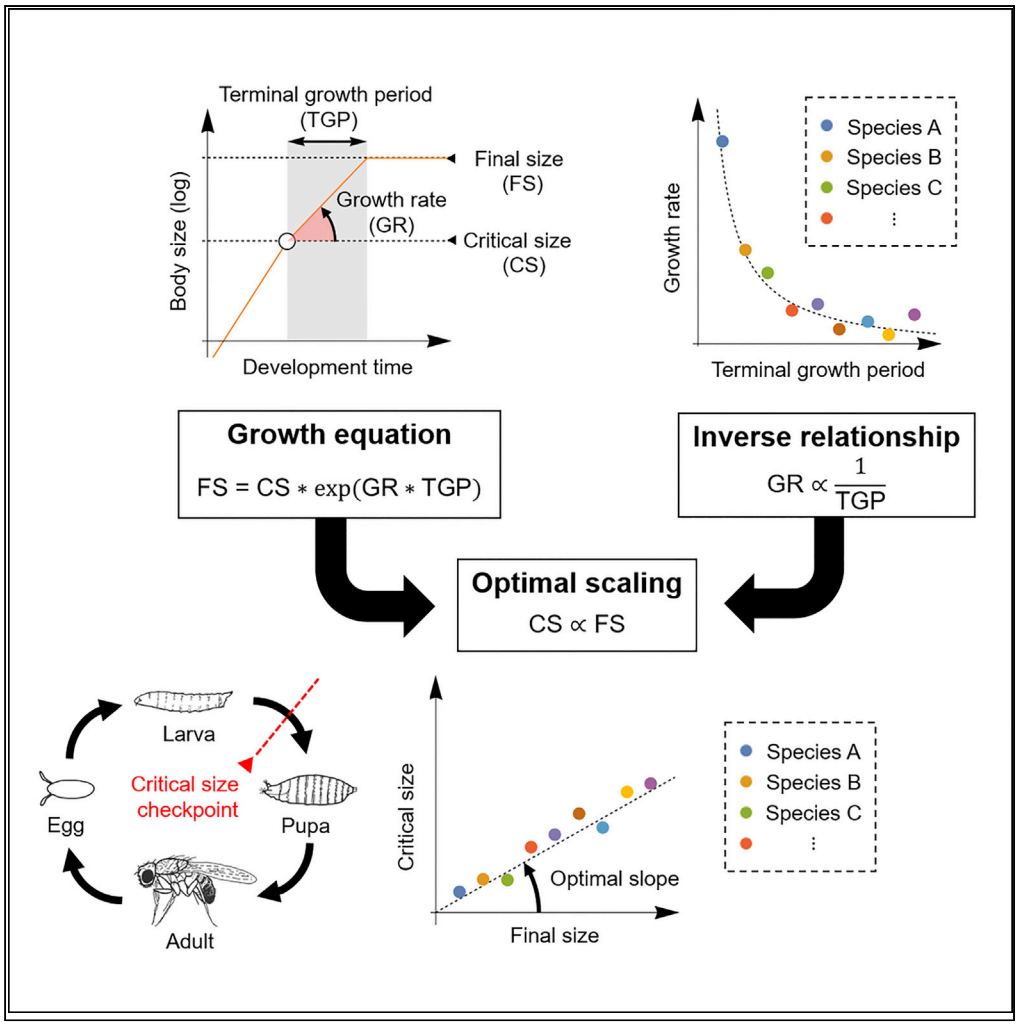

Ken-ichi Hironaka, Koichi Fujimoto, Takashi Nishimura

khironaka@bs.s.u-tokyo.ac.jp (K.-i.H.)
t-nishimura@cdb.riken.jp (T.N.)

HIGHLIGHTS

We quantified the growth parameters including critical size in nine fly species

The optimal scaling of critical size predicted by a life history model is verified

Scaling is explained by an inverse relation between growth duration and growth rate

Species evolution of growth duration can be traced back to that of hormone dynamics

Hironaka et al., iScience *20*, 348–358
October 25, 2019
https://doi.org/10.1016/j.isci.2019.09.033

iScience

CellPress

Article

Optimal Scaling of Critical Size for Metamorphosis in the Genus *Drosophila*

Ken-ichi Hironaka,[1,2,3,4,*] Koichi Fujimoto,[1] and Takashi Nishimura[2,*]

SUMMARY

Juveniles must reach a critical body size to become a mature adult. Molecular determinants of critical size have been studied, but the evolutionary importance of critical size is still unclear. Here, using nine fly species, we show that interspecific variation in organism size can be explained solely by species-specific critical size. The observed variation in critical size quantitatively agrees with the interspecific scaling relationship predicted by the life history model, which hypothesizes that critical size mediates an energy allocation switch between juvenile and adult tissues. The mechanism underlying critical size scaling is explained by an inverse relationship between growth duration and growth rate, which cancels out their contributions to the final size. Finally, we show that evolutionary changes in growth duration can be traced back to the scaling of ecdysteroid hormone dynamics. We conclude that critical size adaptively optimizes energy allocation, and has a central role in organism size determination.

INTRODUCTION

Body size is a common and important trait that affects the physiological and ecological performance of an organism (McMahon and Bonner, 1983; Schmidt-Nielsen, 1984; Thompson, 1942). Although molecular genetics studies have clarified mechanisms controlling organ growth, the mechanisms that determine organism size remain largely unknown because organism growth and organ growth are coordinated but distinct phenomena (Hariharan, 2015; Pan, 2007; Tumaneng et al., 2012). Moreover, given that many animals do not grow indeterminately even with sufficient food, not only growth but also growth cessation is important in determining final size (Boulan et al., 2015; Cook and Tyers, 2007; Edgar, 2006; Gokhale and Shingleton, 2015; Stern, 2003). At the organism level, growth cessation often accompanies a life history transition such as sexual maturation or metamorphosis, which are mediated by the action of hormones such as ecdysteroid hormone (insects), thyroid hormone (amphibians), and sex steroid hormones (mammals). These hormones are usually synthesized only after juveniles reach a certain body size, called the "developmental threshold" or "critical size" (Day and Rowe, 2002). Therefore, the timing of growth cessation is pre-determined upon attainment of critical size, which occurs much earlier than growth cessation (Figure 1). For example, humans enter puberty when reaching a critical body weight and then complete developmental growth and sexual maturation during puberty by the action of sex steroid hormones (Frisch and Revelle, 1971, 1970). Eventually, final body size can be delineated by three factors: critical size, terminal growth period (TGP) between critical size attainment and growth cessation, and growth rate during the TGP (Figure 1).

Previous studies have reported that critical size, TGP, or growth rate can contribute to body size differences at the intraspecific and interstrain level (D'Amico et al., 2001; De Moed et al., 1999; Nijhout et al., 2006; Partridge et al., 1999). This finding presents the question of whether organisms can freely choose between these three size determinants to attain a desirable body size over the course of evolution or if there are principles that govern the evolution of size determinants. To address this issue, it is important to understand the role of critical size in evolution and development. However, critical size has so far been defined directly as a priori physiological constraints without any clear connection to fitness, making it difficult to infer the role of critical size (Day and Rowe, 2002).

Recent studies of holometabolous insects such as *Drosophila* and *Manduca* have provided some insights into the adaptive significance of critical size (Edgar, 2006; Nijhout et al., 2014; Riddiford, 2011). During the larval stage, individuals must reach a critical size to initiate metamorphosis. Attaining critical size induces the prothoracic gland to secrete ecdysteroid hormone, which triggers metamorphic events such as growth cessation and pupation (Koyama et al., 2014; Mirth et al., 2005; Ohhara et al., 2017). In addition, imaginal tissues (i.e., precursors of adult organs) begin rapid growth after attaining critical size in an

[1]Laboratory of Theoretical Biology, Department of Biological Sciences, Osaka University, Osaka 560-0043, Japan

[2]Laboratory for Growth Control Signaling, RIKEN Center for Biosystems Dynamics Research (BDR), Hyogo 650-0047, Japan

[3]Present address: Department of Biological Sciences, Graduate School of Science, University of Tokyo, Tokyo 113-0033, Japan

[4]Lead Contact

*Correspondence: khironaka@bs.s.u-tokyo.ac.jp (K.-i.H.), t-nishimura@cdb.riken.jp (T.N.)

https://doi.org/10.1016/j.isci.2019.09.033

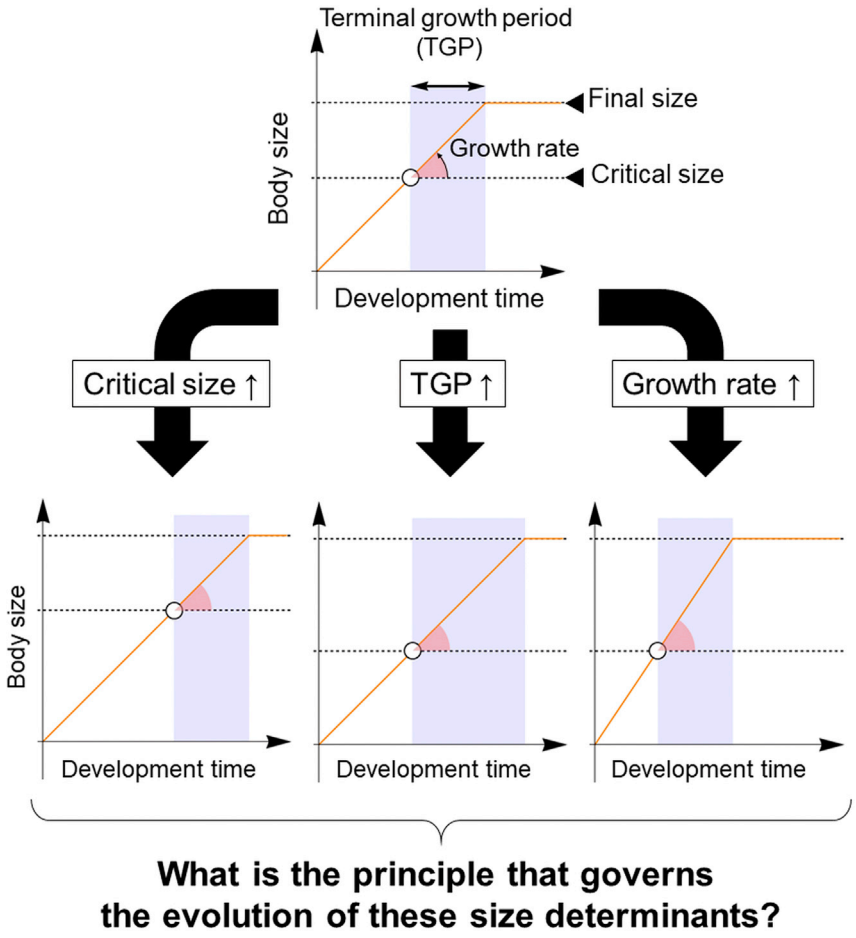

Figure 1. Evolutionary Questions Regarding Developmental Thresholds

In many organisms, adult maturation is triggered by reaching a critical size, also called a developmental threshold. Because there is a lag time between reaching critical size (circle) and growth cessation, the critical size is usually much smaller than the final size. Thus, final body size can be delineated by three factors: critical size (left panel), duration of the terminal growth period (TGP, center panel), and growth rate during the TGP (right panel). Potentially, any of these three determinants can contribute to body size evolution.

ecdysteroid-dependent manner (Bryant and Levinson, 1985; Mirth et al., 2009; Truman et al., 2006). Based on these observations, we hypothesized that critical size mediates an energy allocation switch that slows down the growth of larval tissues and speeds up the growth of adult imaginal tissues (Hironaka and Morishita, 2017). Our model links critical size with fitness and predicts an evolutionary principle for size determination, based on an interspecific scaling relationship between critical size and final larval size (Figure 1C). This scaling relationship is quantitatively testable because the theoretical scaling coefficient is determined solely by two parameters: growth scaling exponent and energy reallocation efficiency.

Here, to test "energy allocation switch" hypothesis of critical size, we examined the interspecific variation in critical size and other growth characteristics using nine *Drosophila* species. Our data confirm that the optimal scaling relationship of critical size holds across the genus *Drosophila*, providing a strong evidence for the energy allocation switch. The mechanism underlying critical size scaling can be explained by an inverse relationship between the growth duration and the growth rate, which cancels out their effects on the final size and makes critical size contribute more directly to the final size. Finally, we show that evolutionary change of the growth duration, or heterochrony, can be traced back to the temporal scaling of ecdysteroid hormone dynamics. Our results suggest that critical size is evolved to optimize energy allocation between different organs, which provides a previously unrecognized principle of organism size evolution.

RESULTS AND DISCUSSION

The Scaling of Critical Size Is Derived from an Optimal Life History Model for Holometabolous Insects

We first introduce the life history model for holometabolous insects and explain how evolution of three size determinants (critical size, TGP, and growth rate) are governed by the optimality principle (see Transparent Methods and Hironaka and Morishita, 2017 for more detailed explanation). The model consists of two state variables: the size of larval tissues, L, and the size of imaginal tissues (precursors of adult organs), I. During the larval stage ($0 < t < t_{CG}$), the organism acquires food from the environment and metabolizes it into energy and materials. Assuming that this process depends only on larval body size, we can write the energy dedicated to growth as $E = gL^k$ (measured in units of body mass per time), where g is the assimilation rate coefficient and k is the growth scaling exponent (Bonduriansky and Day, 2003; Day and Taylor, 1997; Sears and Kerkhoff, 2012; West et al., 2001). The growth energy E is allocated to larval and imaginal tissues according to a controlled ratio, u, which is later optimized (Figure 2A). During the pupal stage ($t_{CG} < t < t_{EC}$), there is no energy influx from the environment to the organism, but imaginal tissues continue to grow using the energy and materials stored in larval tissues, eventually creating the adult body, A_{EC} (Figure 2B). This energy reallocation process is written as $A_{EC} = cL_{CG} + I_{CG}$ where c is the efficiency of energy reallocation.

Under these constraints, when optimizing the energy allocation schedule during the larval stage to maximize adult body size and minimize developmental time, the larval growth pattern inevitably becomes biphasic, due to the bang-bang principle for linear control systems (Hironaka and Morishita, 2017). Specifically, at some time during the larval stage ($t_{CS} \in [0, t_{CG}]$), the growth of larval tissues will slow and the growth of imaginal tissues will speed up (Figure 2C). Because a similar change in growth pattern is observed at the time of critical size attainment *in vivo* (Bryant and Levinson, 1985; Mirth et al., 2009; Truman et al., 2006), we regard the timing of the switch in energy allocation to be the same as the timing of critical size attainment ("critical time"). Therefore, in our model, the late larval growth period after the critical time ($t_{CS} < t < t_{CG}$) corresponds to the terminal growth period (TGP). Although the explicit forms of the critical size $L_{CS} := L(t_{CS})$ and critical time t_{CS} cannot be derived unless the function form of fitness is given, their relative values to the final larval size and to the larval development time can be given, independently of fitness function:

$$L_{CS} = c^{\frac{1}{k}} L_{CG} \quad \text{(Equation 1A)}$$

$$t_{CS} = c^{\frac{1-k}{k}} t_{CG} \quad \text{(Equation 1B)}$$

Thus, only two dimensionless parameters, growth scaling exponent k and energy reallocation efficiency c, determine the relative values of critical size and critical time. Equation 1 insists that the critical size and critical timescale proportionally with the final larval size and larval development time, respectively, as long as the values of k and c are conserved among focal species. Therefore, we refer to these equations as the "optimal scaling." The optimal scaling relationship represents a guiding principle for three size determinants: critical size, TGP, and growth rate. A simpler expression of this relationship is derived under the assumption that growth is exponential during TGP, which is often used in other studies (Nijhout et al., 2006; Shingleton et al., 2008; Vollmer et al., 2016):

$$[\text{TGP}] \propto [\text{Growth rate}]^{-1} \quad \text{(Equation 2)}$$

where [TGP] is the duration of TGP and [Growth rate] is the exponential growth rate during the TGP. The detailed derivation of Equation 2 is described in Transparent Methods. This inversely proportional relationship between TGP and growth rate provides insight into the physiological mechanisms by which organisms optimize the energy allocation schedule during evolution, as discussed in detail later.

The Optimal Scaling of Critical Size Is Experimentally Validated in the Genus *Drosophila*

A key question concerns whether critical size, TGP, and growth rate are freely determined or governed by the optimal scaling. To this end, we measured interspecific variation in critical size and other growth parameters in nine *Drosophila* species and checked the following three conditions: (1) the proportional relationship between critical size (L_{CS}) and final larval size (L_{CG}), (2) the constancy of k and c between species, and (3) the consistency between the observed proportionality constant (L_{CS}/L_{CG}) and the predicted proportionality constant ($c^{1/k}$). Flies used in experiments were from five species of the subgenus Sophophora

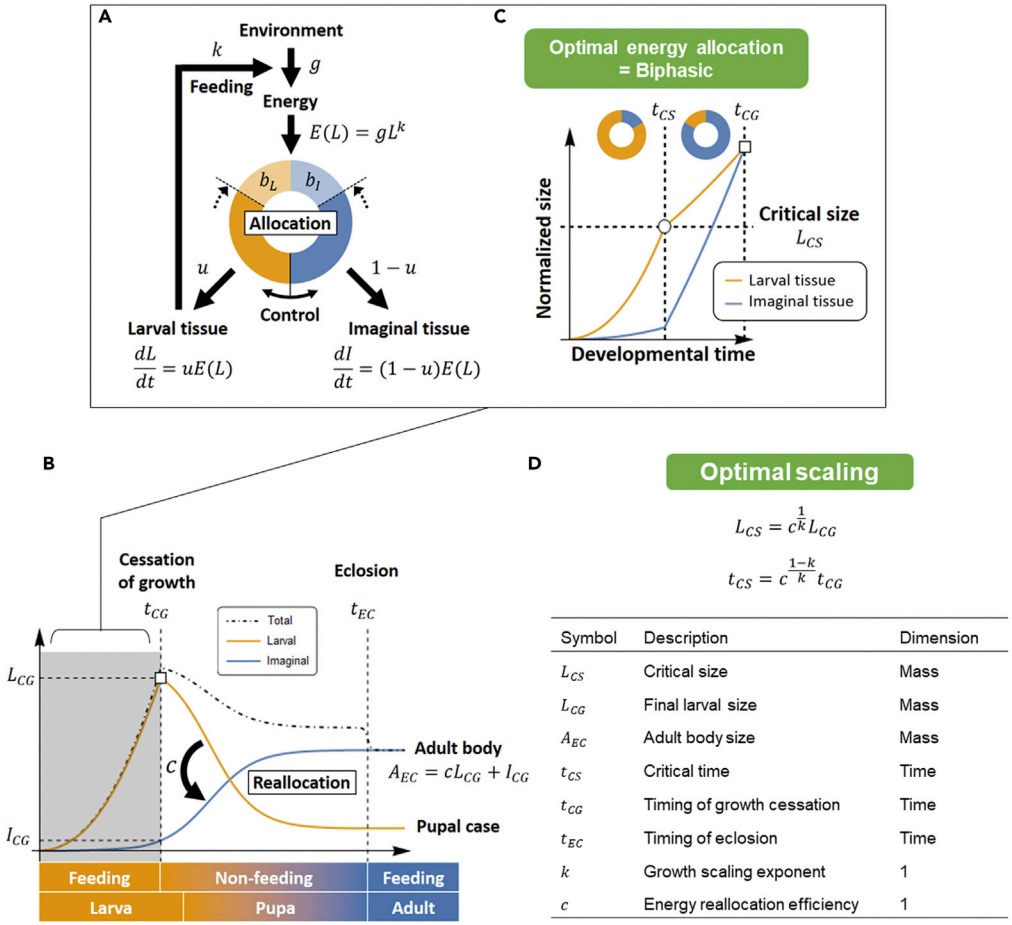

Symbol	Description	Dimension
L_{CS}	Critical size	Mass
L_{CG}	Final larval size	Mass
A_{EC}	Adult body size	Mass
t_{CS}	Critical time	Time
t_{CG}	Timing of growth cessation	Time
t_{EC}	Timing of eclosion	Time
k	Growth scaling exponent	1
c	Energy reallocation efficiency	1

Figure 2. Optimal Life History Model for Holometabolous Insects

(A) During the larval stage ($t \in [0, t_{CG}]$), the larva acquires energy (E) from the environment in a larval body size-dependent manner ($E(L) = gL^k$) and allocates it to the growth of the larval (L, orange) and imaginal tissue (I, blue) according to the ratio $u(t)$:$1 - u(t)$ and under the constraint $u \in [b_L, 1-b_I]$ (see Transparent Methods for details).

(B) During the pupal stage ($t \in [t_{CG}, t_{EC}]$), there is no feeding and therefore no energy influx from the environment to the pupa. But the imaginal tissues continue growing using energy stored in larval tissues, eventually becoming the body structures of the mature adult. Representing the efficiency with c, this energy reallocation process is written as $A_{EC} = cL_{CG} + I_{CG}$.

(C) When maximizing fitness (e.g., adult body size) using the bang-bang principle for linear control systems, the energy allocation during the larval stage becomes biphasic: earlier larval growth and later imaginal growth (see Transparent Methods for details). We regard the phase-transition point as the critical size (or critical time; circle).

(D) Scaling relationship derived from the optimal life history model. Meanings of variables and parameters are shown in the lower table.

(*D. melanogaster*, *D. simulans*, *D. atripex*, *D. willistoni*, and *D. pseudoobscura*) and four species of the subgenus Drosophila (*D. mercatorum*, *D. repleta*, *D. virilis*, and *D. quadrilineata*) (Figure 3A).

First, to check the proportional relationship, we measured the final larval size and the critical size for each species. When nine species were raised in a 25°C incubator with a common standard diet, they grew to be normal adults, although development speeds differed between species (Figures 3B and S1). At the timing of growth cessation (t_{CG}), we observed interspecific variation in the final larval size L_{CG} of up to 3-fold (Figures 3B and 3C). Next, critical size L_{CS} was measured by starvation experiments (see Methods and Transparent Methods for details). In *Drosophila*, the "minimal viable weight," a size below which animals cannot survive starvation to pupariate, is often used as a proxy for critical size (method A—Mirth et al., 2005; De Moed et al., 1999; Ohhara et al., 2017). Alternatively, the "breakpoint" in a plot of larval mass at starvation versus time to pupariation, namely, a size below which larvae pupariate with a significant delay, is defined

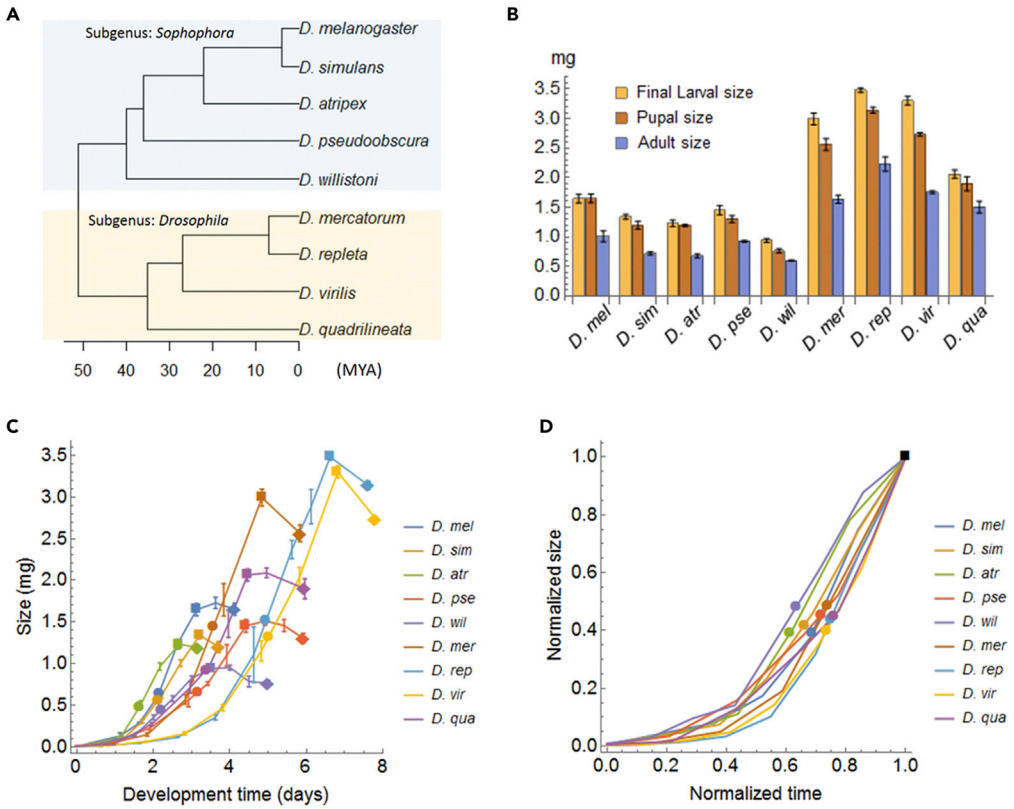

Figure 3. Growth Profiles of the Nine *Drosophila* Species

(A) Phylogenetic tree of *Drosophila* species in this study. Branch length indicates evolutionary divergence time, obtained by integrating published data (Grath et al., 2009; Katoh et al., 2007; Song et al., 2011).

(B) Larval, pupal, and adult size of the nine species (sampled at growth cessation, pupariation, and eclosion, respectively). Error bars represent standard errors of the mean (n = 3–10 batches).

(C) Larval growth curves of the nine *Drosophila* species. After the time of growth cessation (squares), larvae enter the non-feeding/wandering period, leading to pupariation (diamonds). Filled circles indicate the timing of critical size attainment. Error bars represent standard errors of the mean (n = 3–10 batches).

(D) All larval growth curves and positions of critical size attainment (filled circles) were mostly overlapping when normalized by the maximal points (square).

as critical size in several studies (method B—Callier et al., 2013; Ghosh et al., 2013; Stieper et al., 2008; Testa et al., 2013). To examine both methods, we obtained the pupariation rate and pupariation time as functions of the larval size at starvation and calculated the critical size for each species in two different ways (Figures S2 and S3). Both methods provided quantitatively similar results ($r = 0.99$, Pearson's correlation coefficient; Figure S3C); therefore, here we show results of the former method, unless otherwise mentioned.

We found that critical size had an interspecific variation of up to 3-fold, similar to the final larval size (Figures 3C and 3D), and confirmed a proportional relationship between critical size and final larval size ($L_{CS} = 0.44 * L_{CG}, R^2 = 0.99$; blue dashed line in Figure 4A; see Figure S4A for method B), as well as between the critical time and the larval development time ($t_{CS} = 0.72 * t_{CG}, R^2 = 0.99$; blue dashed line in Figure 4B; see Figure S4B for method B). Interestingly, the critical size of the largest species (*D. repleta*) was larger than the final larval size of the smallest species (*D. willistoni*), although larval morphologies of these species are almost indistinguishable. This observation suggests that the critical size is determined not by mechanical limit but by evolutionary consequences.

Second, to check the constancy of k and c between species, we estimated these parameters for each species by measuring the ontogenetic growth curve. We determined k by fitting the larval growth curve with a power law for each species (see Transparent Methods; Figure S1D). All larval growth curves were mostly overlapping when normalized by their maximal points, which indicates small k variation (Figure 3D). Indeed,

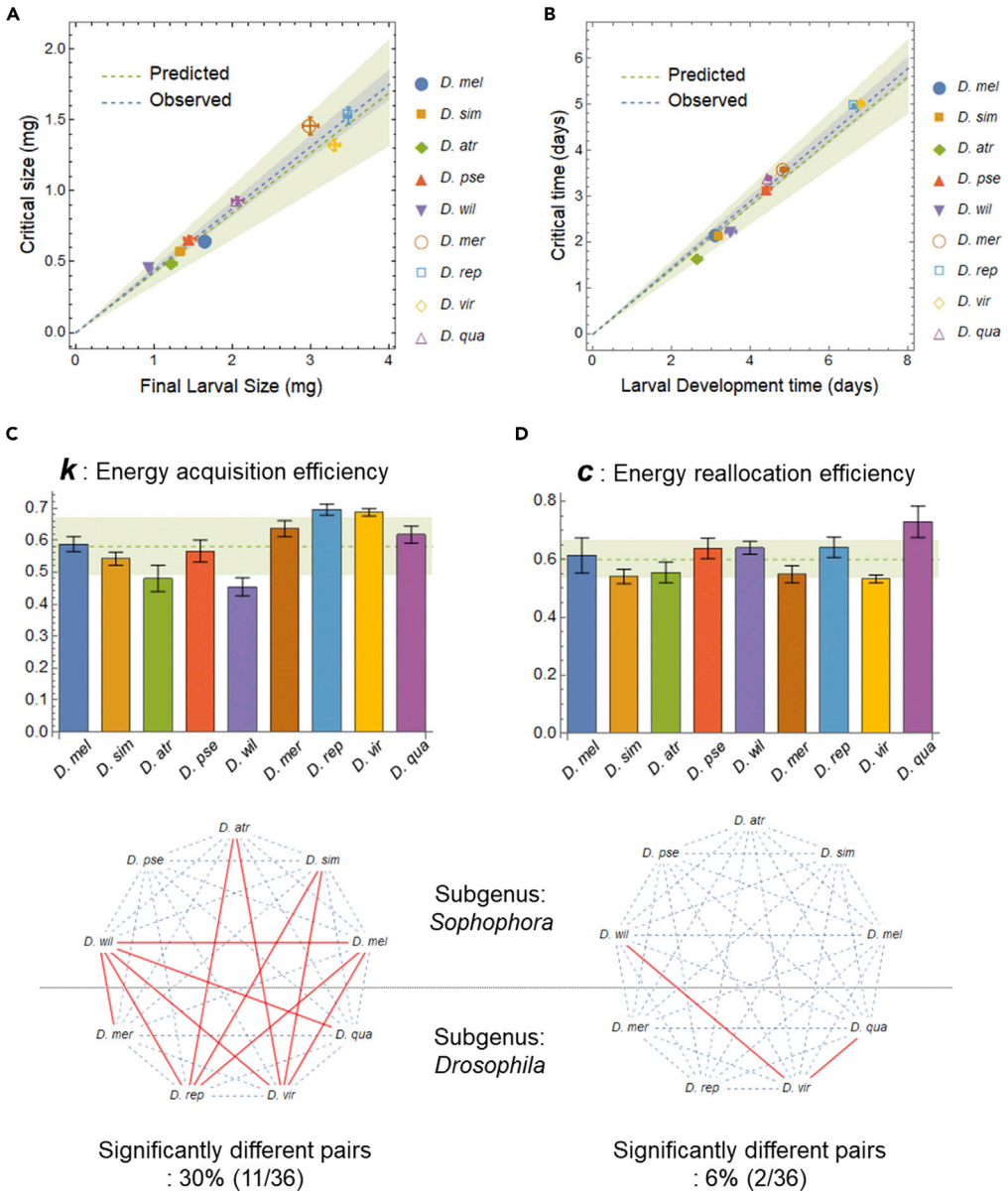

Figure 4. Optimal Scaling of Critical Size and Critical Time

(A and B) Scaling relationships between critical size and final larval size (A) and between the larval development time and the critical time (B). Blue lines show the regression lines fitted by the linear model without an offset (blue shaded area: 95% CI), whereas green lines show the theoretical lines predicted by the life history model using the average of c and k from nine *Drosophila* species (green shaded area: standard deviation between the nine species). Here we used method A to calculate critical size.

(C and D) Interspecific comparison of parameters for energy acquisition efficiency k (C) and for energy reallocation efficiency c (D). Error bars are the standard errors calculated by the law of propagation of uncertainty. In the background, mean (dashed lines) and $\pm$SD (shaded area) of nine species are shown. In lower panels, significantly different pairs are connected by red lines (pairwise z-test comparisons with Bonferroni correction at a significance of $\alpha = 0.01$). Most of the significantly different pairs cross the border of subgenus indicated by the black dashed line.

interspecific differences in the value of k were non-significant for 70% of all possible pairs (25/36, pairwise z-test comparisons; Figure 4C). Next, we obtained c from the ratio of the final larval size to the adult size at eclosion (see Transparent Methods; Figure 3B). Despite substantial variation in body size, interspecific differences for c values were non-significant for 94% of all possible pairs (34/36, pairwise z-test; Figure 4D). For both k and c, which had ranges of possible values between 0 and 1, the intra-genus variations were less

than 10%: k = 0.58 ± 0.09, c = 0.6 ± 0.07 (mean ± SD of nine species; Figures 4C and 4D). Thus, we concluded that both k and c can be regarded as almost constant between species. These results led us to expect that the optimal scaling of critical size is valid in these species.

Third, to check the consistency between the observed proportionality constant (L_{CS}/L_{CG}) and the predicted proportionality constant ($c^{1/k}$), we calculated the latter value by using the average values of k and c of nine *Drosophila* species and compared it with the former value, which is already calculated previously. For the scaling relationship of critical size indicated by Equation 1A, the predicted constant was: $c^{1/k}$ = 0.42 ± 0.09 (mean ± SD of nine species; the green dashed line and shaded region in Figures 4A and S4A), which was quantitatively consistent with the observed constant: L_{CS}/L_{CG} = 0.44 ± 0.03 (mean ± 95% confidence interval [CI]; Figure 4A). For the scaling relationship of critical time indicated by Equation 1B, the predicted constant was: $c^{(1-k)/k} = 0.7 \pm 0.1$ (mean ± SD of nine species; the green dashed line and shaded region in Figures 4B and S4B), which was also close to the observed constant: t_{CS}/t_{CG} = 0.72 ± 0.03 (mean ± 95% CI; Figure 4B). Finally, for all pairs of the observed constant and the predicted constant (for critical size or critical time; for method A or method B), we performed equivalence tests using two one-sided z-tests (Hatch, 1996). In each of the four comparisons, the null hypothesis $|\Delta x| > \delta$ was rejected at a significance level of 0.01, where $\Delta x := x_{\text{observed}} - x_{\text{predicted}}$ is the difference between observation and prediction and δ is the standard deviation of $x_{\text{predicted}}$ (the standard error of x_{observed} was used as that of Δx). These results indicate that the observed values are within the theoretically expected range: $x_{\text{predicted}} - \delta \leq x_{\text{observed}} \leq x_{\text{predicted}} + \delta$.

We should note that, even if we assume that the proportionality constants differ between species, observed values for relative critical size and for relative critical time show good agreement with the predicted values (Figures S4C and S4D).

Taken together, we confirmed (1) the proportional relationship, (2) the constancy of c and k, and (3) the consistency between the observed proportionality constant and the predicted proportionality constant. These results indicate that the life history model is accurate to experimental observations, at least in the genus *Drosophila*, and suggest that size determinants, including critical size, TGP, and growth rate, are constrained by the optimal scaling.

The Scaling of Critical Size Is Achieved by an Evolutionary Change that Inversely Correlates Growth Duration and Growth Rate

As explained earlier, the inversely proportional relationship between TGP and growth rate is theoretically derived from the optimal scaling between critical size and final size. Indeed, we observed a strong negative correlation between the TGP and growth rate ($r = -0.85$; Figure 5A), which can be accurately approximated by the inverse proportionality: $[\text{TGP}] = 0.82 * [\text{Growth rate}]^{-1}$ (Figure 5A). From these observations, we can infer that, during evolution, organisms optimized the energy allocation schedule by adaptively changing TGP for the species-specific growth rate.

Then, we asked what molecular mechanisms determine the interspecific difference in the TGP. Because the duration of TGP (or the timing of growth cessation) is regulated by ecdysteroid (Yamanaka et al., 2013), we investigated the dynamics of ecdysteroid titer in three flies that had marked differences in TGP duration (*D. melanogaster, D. willistoni, D. virilis*). We also measured growth curves for the wing imaginal disc as another index of developmental progression. All species had exponential increases in both ecdysteroid titer and growth of the imaginal disc after reaching critical size (Figure 5B), consistent with our model's predictions (Figure 1C). There was clear interspecific variation in the rate of increase of ecdysteroid titer, which positively correlated with the TGP duration; the species with a shorter TGP had faster rates of ecdysteroid increase. These results imply that the change in hormone dynamics caused the change in developmental rate during divergence of these species (i.e., heterochrony).

Finally, we asked which molecular mechanisms underlie the correlation between the ecdysteroid synthesis rate and growth rate. It is possible that this correlation is due to a built-in mechanism in *Drosophila*, because a negative correlation between TGP and the growth rate is also observed in sexual dimorphism (Testa et al., 2013) and many types of phenotypic plasticity in response to temperature (Ghosh et al., 2013), oxygen (Callier et al., 2013), and nutrition (Layalle et al., 2008). In particular, Layalle et al. (2008) reported that larvae reared with low nutrition had a decreased growth rate and an increased TGP, both of

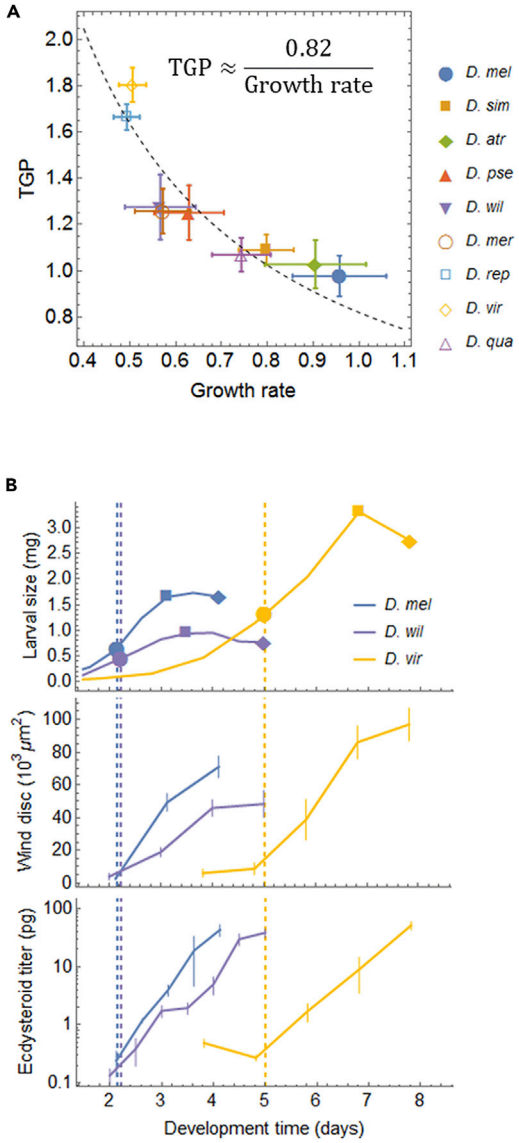

Figure 5. Mechanisms Underlying the Optimal Scaling of Critical Size

(A) In the nine species, there is a negative correlation between the growth rate and the duration of TGP, which ensures the scaling between critical size and final size. The dashed curve indicates the nonlinear regression fit ($y = 0.82/x$). Error bars are standard error calculated by the law of propagation of uncertainty.

(B) For the three species with marked differences in the TGP duration (*D. mel*, *D. wil*, *D. rep*), growth curves of larval body (upper panel) and wing imaginal disc (middle panel) and temporal profiles of ecdysteroid titer (lower panel) are shown. Filled circles, squares, and diamonds indicate the timing of critical size attainment, growth cessation, and pupariation, respectively. Error bars represent standard deviations (n = 3–6 batches).

which are regulated by insulin/insulin-like growth factor signaling (IIS) and/or TOR signaling (Layalle et al., 2008): a systemic decrease in IIS and/or TOR signaling downregulates the organismal growth rate through peripheral tissues, including the imaginal disc and fat body. In contrast, decreased IIS and/or TOR signaling in the prothoracic gland that governs ecdysteroid production prolongs the duration of TGP. Thus, because IIS and/or TOR signaling can inversely regulate growth rate and growth duration, these may serve as an underlying mechanism for scaling critical size during evolution. Although optimal scaling in a broad sense (indicated by Equation 1) cannot predict which of three size determinants contribute to final size evolution, if such a built-in scaling mechanism is conserved across species, critical size would be a main driver of final size evolution. Future work should compare the intensity of insulin

signaling between different species and clarify the potential roles of IIS and/or TOR signaling in critical size scaling and final size determination.

Applicable Scope of the Optimal Scaling and Energy Allocation Switch

The high coefficient of determination (R^2 = 0.99 in Figures 4A and 4B) in the optimal scaling relationship indicates that body size difference at the interspecific level can be explained solely by the critical size. The inverse relationship between TGP and growth rate clearly explains why these two factors do not contribute to body size difference, whereas their values differ between species: the opposite directions of their variation cancel out each other's effect on final size. Although this is seemingly contrary to the conventional view that critical size, TGP, or growth rate can contribute to the determining final size (D'Amico et al., 2001; De Moed et al., 1999; Nijhout et al., 2006; Partridge et al., 1999), it is a matter of scale: if the genetic distance is too small, it would be difficult to recognize the scaling relationship because the size variation would be too small. Conversely, if the genetic distance is too large, the scaling relationship would not hold because physiological parameters such as *c* and *k* can differ between species. What we observe from an interspecies or interstrain comparison can change depending on the focal scale of evolutionary time or genetic distance.

Limitation of This Study

We should note that not all holometabolous insects commit to becoming pupae in a manner dependent on critical size, like *Drosophila*. In some beetles and solitary bees, critical size does not seem to exist and pupation is triggered by food deprivation or starvation (Helm et al., 2017; Nagamine et al., 2016; Nijhout, 2008). Even in *Manduca sexta*, which does have a critical size, the pupation mechanism has several physiological features that are distinct from *Drosophila* (e.g., inhibitory effect of juvenile hormone on pupation, log-linear relationship between molting size and critical size; please see Transparent Methods and Figure S5 for details). These observations suggest that the pupal commitment mechanisms are very diverse between species, but the concept of an energy allocation switch can be applied more broadly across species and apart from critical size. Even in insects without a critical size, the pupal commitment determining final body size may still be closely linked to an energy allocation switch (Figure 2).

Conclusion

Our data show that the critical sizes of nine *Drosophila* species follow a scaling relationship that is derived from an optimal energy allocation model. Furthermore, we find that an inverse correlation between growth rate and growth duration, which is caused by temporal scaling of hormone dynamics, cancels out their effects on the final size and makes critical size contribute more directly to the final size. These findings emphasize the central role of critical size in size determination and suggest a common principle for the evolution of organism size. Similar principles may be found in organisms other than holometabolous insects by developing an energy allocation model that accounts for organism-specific life history.

METHODS

All methods can be found in the accompanying Transparent Methods supplemental file.

SUPPLEMENTAL INFORMATION

Supplemental Information can be found online at https://doi.org/10.1016/j.isci.2019.09.033.

ACKNOWLEDGMENTS

We thank M. Watada and EHIME-Fly, the laboratory for Drosophila resources at Ehime University, for fly stocks and N. Okamoto, Y. Morishita, K. Matsushita, and A. Shingleton for fruitful discussion and useful hints. This work was supported in part by Scientific Research Grants from MEXT to T.N. (17H03658, 17K19433) and K.F. (17H06386) and by Grant-in-Aid for JSPS Fellows to K.H. (15J04931).

AUTHOR CONTRIBUTIONS

K.H. and T.N. designed and performed the experiments. K.H. analyzed the data, conducted the mathematical modeling, and wrote the original manuscript. K.F. and T.N. supervised the project and reviewed and edited the manuscript.

DECLARATION OF INTERESTS

The authors declare no competing financial interests.

Received: March 4, 2019
Revised: July 19, 2019
Accepted: September 23, 2019
Published: October 25, 2019

REFERENCES

Bonduriansky, R., and Day, T. (2003). The evolution of static allometry in sexually selected traits. Evolution *57*, 2450–2458.

Boulan, L., Milán, M., and Léopold, P. (2015). The systemic control of growth. Cold Spring Harb. Perspect. Biol. *7*, https://doi.org/10.1101/cshperspect.a019117.

Bryant, P.J., and Levinson, P. (1985). Intrinsic growth control in the imaginal primordia of Drosophila, and the autonomous action of a lethal mutation causing overgrowth. Dev. Biol. *107*, 355–363.

Callier, V., Shingleton, A.W., Brent, C.S., Ghosh, S.M., Kim, J., and Harrison, J.F. (2013). The role of reduced oxygen in the developmental physiology of growth and metamorphosis initiation in *Drosophila melanogaster*. J. Exp. Biol. *216*, 4334–4340.

Cook, M., and Tyers, M. (2007). Size control goes global. Curr. Opin. Biotechnol. *18*, 341–350.

D'Amico, L.J., Davidowitz, G., and Nijhout, H.F. (2001). The developmental and physiological basis of body size evolution in an insect. Proc. R. Soc. Lond. B Biol. Sci. *268*, 1589–1593.

Day, T., and Rowe, L. (2002). Developmental thresholds and the evolution of reaction norms for age and size at life-history transitions. Am. Nat. *159*, 338–350.

Day, T., and Taylor, P.D. (1997). Von Bertalanffy's growth equation should not be used to model age and size at maturity. Am. Nat. *149*, 381–393.

De Moed, G.H., Kruitwagen, C.L.J.J., De Jong, G., and Scharloo, W. (1999). Critical weight for the induction of pupariation in *Drosophila melanogaster*: genetic and environmental variation. J. Evol. Biol. *12*, 852–858.

Edgar, B.A. (2006). How flies get their size: genetics meets physiology. Nat. Rev. Genet. *7*, 907–916.

Frisch, R.E., and Revelle, R. (1971). Height and weight at menarche and a hypothesis of menarche. Arch. Dis. Child. *46*, 695–701.

Frisch, R.E., and Revelle, R. (1970). Height and weight at menarche and a hypothesis of critical body weights and adolescent events. Science *169*, 397–399.

Ghosh, S.M., Testa, N.D., and Shingleton, A.W. (2013). Temperature-size rule is mediated by thermal plasticity of critical size in *Drosophila melanogaster*. Proc. Biol. Sci. *280*, 20130174.

Gokhale, R.H., and Shingleton, A.W. (2015). Size control: the developmental physiology of body and organ size regulation. Wiley Interdiscip. Rev. Dev. Biol. *4*, 335–356.

Grath, S., Baines, J.F., and Parsch, J. (2009). Molecular evolution of sex-biased genes in the *Drosophila ananassae* subgroup. BMC Evol. Biol. *9*, 291.

Hariharan, I.K. (2015). Organ size control: lessons from Drosophila. Dev. Cell *34*, 255–265.

Hatch, J.P. (1996). Using statistical equivalence testing in clinical biofeedback research. Biofeedback Self. Regul. *21*, 105–119.

Helm, B.R., Rinehart, J.P., Yocum, G.D., Greenlee, K.J., and Bowsher, J.H. (2017). Metamorphosis is induced by food absence rather than a critical weight in the solitary bee, *Osmia lignaria*. Proc. Natl. Acad. Sci. U S A *114*, 10924–10929.

Hironaka, K., and Morishita, Y. (2017). Adaptive significance of critical weight for metamorphosis in holometabolous insects. J. Theor. Biol. *417*, 68–83.

Katoh, T., Nakaya, D., Tamura, K., and Aotsuka, T. (2007). Phylogeny of the *Drosophila immigrans* species group (Diptera: Drosophilidae) based on *Adh* and *Gpdh* sequences. Zool. Sci. *24*, 913–921.

Koyama, T., Rodrigues, M.A., Athanasiadis, A., Shingleton, A.W., and Mirth, C.K. (2014). Nutritional control of body size through FoxO-Ultraspiracle mediated ecdysone biosynthesis. Elife *3*, e03091.

Layalle, S., Arquier, N., and Léopold, P. (2008). The TOR pathway couples nutrition and developmental timing in Drosophila. Dev. Cell *15*, 568–577.

McMahon, T., and Bonner, J. (1983). On Size and Life (Scientific American Books).

Mirth, C., Truman, J.W., and Riddiford, L.M. (2005). The role of the prothoracic gland in determining critical weight for metamorphosis in *Drosophila melanogaster*. Curr. Biol. *15*, 1796–1807.

Mirth, C.K., Truman, J.W., and Riddiford, L.M. (2009). The ecdysone receptor controls the post-critical weight switch to nutrition-independent differentiation in Drosophila wing imaginal discs. Development *136*, 2345–2353.

Nagamine, K., Ishikawa, Y., and Hoshizaki, S. (2016). Insights into how longicorn beetle larvae determine the timing of metamorphosis: starvation-induced mechanism revisited. PLoS One *11*, e0158831.

Nijhout, H.F. (2008). Size matters (but so does time), and it's OK to be different. Dev. Cell *15*, 491–492.

Nijhout, H.F., Davidowitz, G., and Roff, D.A. (2006). A quantitative analysis of the mechanism that controls body size in *Manduca sexta*. J. Biol. *5*, 16.

Nijhout, H.F., Riddiford, L.M., Mirth, C., Shingleton, A.W., Suzuki, Y., and Callier, V. (2014). The developmental control of size in insects. Wiley Interdiscip. Rev. Dev. Biol. *3*, 113–134.

Ohhara, Y., Kobayashi, S., Yamanaka, N., Kaynig, V., Longair, M., and Pietzsch, T. (2017). Nutrient-dependent endocycling in steroidogenic tissue dictates timing of metamorphosis in *Drosophila melanogaster*. PLoS Genet. *13*, e1006583.

Pan, D. (2007). Hippo signaling in organ size control. Genes Dev. *21*, 886–897.

Partridge, L., Langelan, R., Fowler, K., Zwaan, B., and French, V. (1999). Correlated responses to selection on body size in *Drosophila melanogaster*. Genet. Res. *74*, 43–54.

Riddiford, L.M. (2011). When is weight critical? J. Exp. Biol. *214*, 1613–1615.

Schmidt-Nielsen, K. (1984). Scaling: Why Is Animal Size So Important? (Cambridge University Press).

Sears, K., and Kerkhoff, A. (2012). Ontogenetic scaling of metabolism, growth, and assimilation: testing metabolic scaling theory with *Manduca sexta* larvae. Physiol. Biochem. Zool. *85*, 159–173.

Shingleton, A.W., Mirth, C.K., and Bates, P.W. (2008). Developmental model of static allometry in holometabolous insects. Proc. Biol. Sci. *275*, 1875–1885.

Song, X., Goicoechea, J.L., Ammiraju, J.S.S., Luo, M., He, R., Lin, J., Lee, S.-J., Sisneros, N., Watts, T., Kudrna, D.A., et al. (2011). The 19 genomes of Drosophila: a BAC library resource for genus-wide and genome-scale comparative evolutionary research. Genetics *187*, 1023–1030.

Stern, D. (2003). Body-size control: how an insect knows it has grown enough. Curr. Biol. *13*, R267–R269.

Stieper, B.C., Kupershtok, M., Driscoll, M.V., and Shingleton, A.W. (2008). Imaginal discs regulate developmental timing in *Drosophila melanogaster*. Dev. Biol. *321*, 18–26.

Testa, N.D., Ghosh, S.M., and Shingleton, A.W. (2013). Sex-specific weight loss mediates sexual size dimorphism in *Drosophila melanogaster*. PLoS One *8*, e58936.

Thompson, D.W. (1942). On Growth and Form (Cambridge Univ. Press).

Truman, J.W., Hiruma, K., Allee, J.P., Macwhinnie, S.G.B., Champlin, D.T., and Riddiford, L.M. (2006). Juvenile hormone is required to couple imaginal disc formation with nutrition in insects. Science *312*, 1385–1388.

Tumaneng, K., Russell, R.C., and Guan, K.-L. (2012). Organ size control by Hippo and TOR pathways. Curr. Biol. *22*, R368–R379.

Vollmer, J., Iber, D., Ahuja, C., Eswaran, H., and Nijhout, H.F. (2016). An unbiased analysis of candidate mechanisms for the regulation of Drosophila wing disc growth. Sci. Rep. *6*, 39228.

West, G.B., Brown, J.H., and Enquist, B.J. (2001). A general model for ontogenetic growth. Nature *413*, 628–631.

Yamanaka, N., Rewitz, K.F., and O'Connor, M.B. (2013). Ecdysone control of developmental transitions: lessons from Drosophila research. Annu. Rev. Entomol. *58*, 497–516.

ISCI, Volume *20*

Supplemental Information

Optimal Scaling of Critical Size for Metamorphosis in the Genus *Drosophila*

Ken-ichi Hironaka, Koichi Fujimoto, and Takashi Nishimura

Supplementary figures

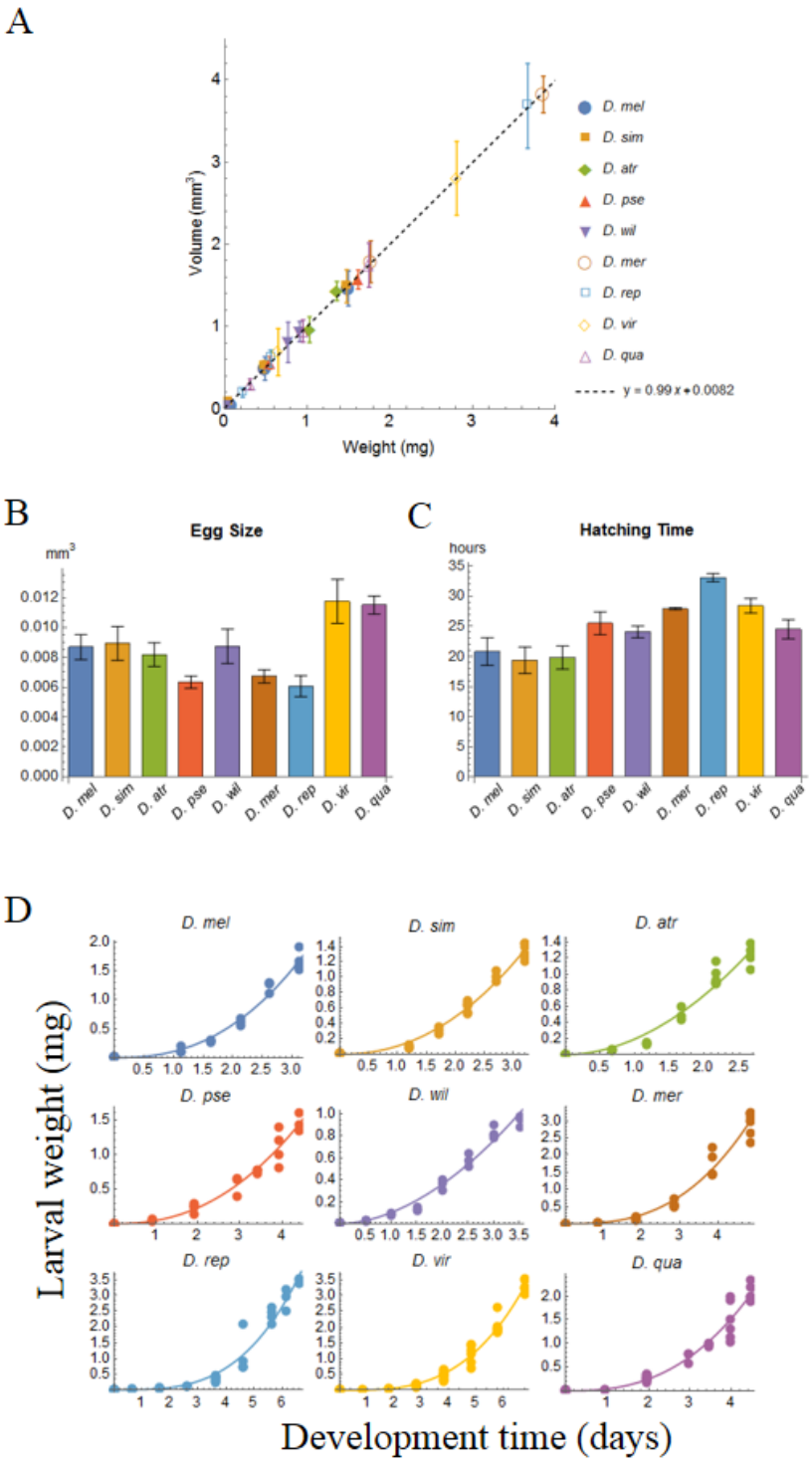

Figure S1. Egg size and hatching time of the nine *Drosophila* species, related to Figure 3.

(A) Larval weight (mg) vs. larval volume (mm^3). Data points around the diagonal $(y=x)$ indicates that the density of larvae is almost the same as the density of water ($1\ g/cm^3\ = 1\ mg/mm^3$). Error bars represent the standard deviations (n = 10). **(B)** Egg volume (V) estimated by the formula of a prolate spheroid: $V = 4/3\pi(L/2)(l/2)^2$ (L is the length and l is the width of egg, measured under the microscope). Error bars represent standard deviations (n = 10–21). **(C)** Hatching time measured by time-lapse imaging of eggs reared at 25°C. Error bars represent standard deviations (n = 12–48). **(D)** Fitting of growth curve (from hatching until growth cessation) with a power function $y = ax^b$. The values of parameter k are obtained by $k = 1 - 1/b$.

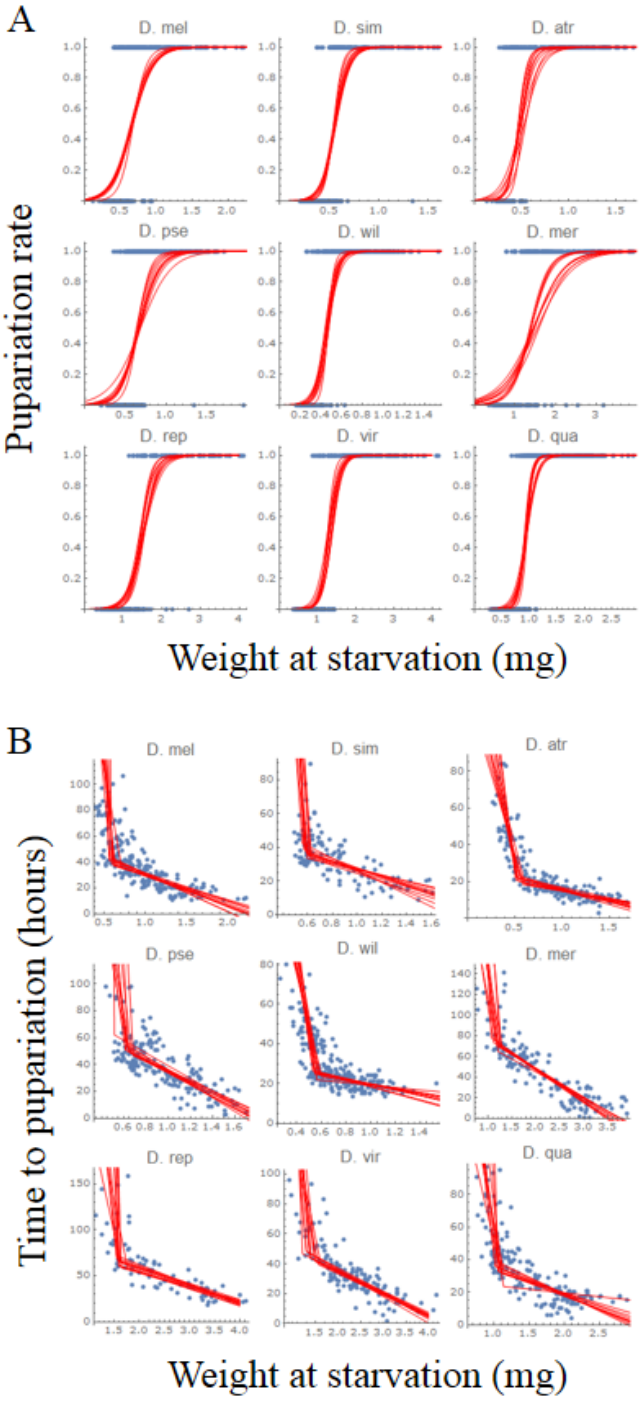

Figure S2. Estimation of critical size, related to Figures 3 and 4.

(A) Method A: logistic regression of the pupariation rate (0 = not pupariated, 1 = pupariated) vs. the weight at starvation. In the regression curves, the weight at which 50% of larvae pupated corresponded to the points at which larvae reached critical size. Regression curves (red) for 10 of the 1000 bootstrapped samples are superimposed on raw data (blue dots). **(B)** Method B: a segmented linear regression of the time to pupariation vs. the weight at starvation. The breakpoints in the regression

lines corresponded to the points at which larvae reached critical size. Regression lines (red) for 10 of the 1000 bootstrapped samples are superimposed on raw data (blue dots).

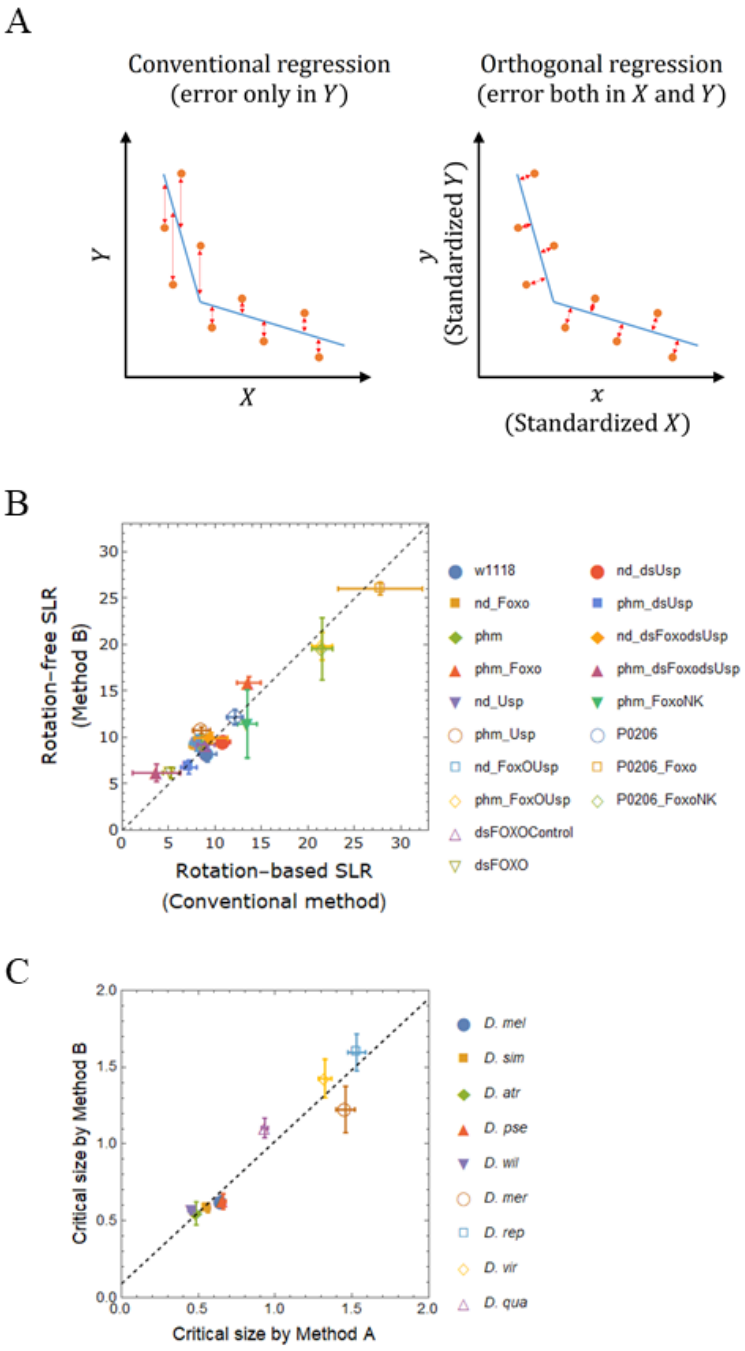

Figure S3. Rotation-free segmented linear regression, related to Figures 3 and 4.

(A) The conventional segmented linear regression considers the errors only in the y-axis (left panel), whereas our method considers the errors in both the x- and y-axes (right panel). **(B)** Breakpoint comparison calculated by two different methods: horizontal axis, rotation-based SLR proposed in previous study (Callier et al., 2013; Ghosh et al., 2013; Testa et al., 2013); vertical axis, rotation-free SLR proposed in this study. Because points appear around the diagonal line for all genotypes, we can see that the method returns almost the same result as the conventional method. Here we used the

published data from the previous study on critical size (Koyama et al., 2014). In this plot, both x and y indicate critical time (hours after L3 ecdysis). **(C)** Comparison of critical weight of nine Drosophila species between methods A and B. The dashed line calculated by linear regression $(0.9x + 0.09)$ represents a significant correlation ($r = 0.96; P < 0.01$).

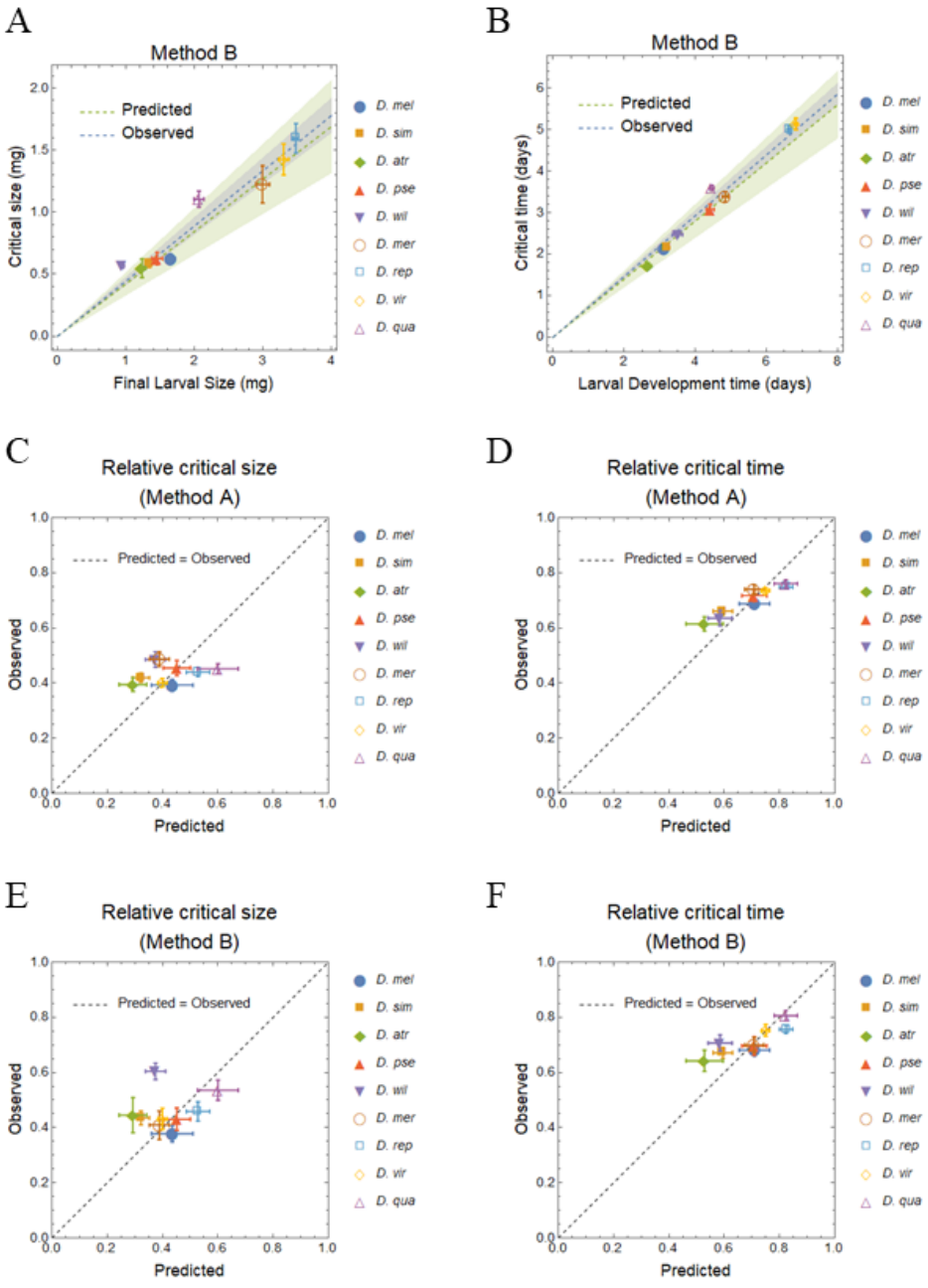

Figure S4. Scaling relationships of critical size and critical time, related to Figures 3 and 4.
(A and B) Scaling relationships between critical size and final larval size (A), and between the larval development time and the critical time (B). Blue lines show the regression lines fitted by the linear

model without an offset [$L_{CS} = 0.45\ L_{CG}$ for (A) and $t_{CS} = 0.73\ t_{CG}$ for (B); shaded area: 95% CI], whereas green lines show the same result as Figure 4A and B. Here we used method B to calculate critical size. **(C and D)** Comparison of relative critical size (C) or relative critical time (D) between prediction based on method A and experimental observation. **(E and F)** Comparison of relative critical size (E) or relative critical time (F) according to prediction based on method B and experimental observation. In both methods, relative critical size showed weak correlation (method A: 0.24, method B: 0.21) and relative critical time showed strong correlation (method A: 0.95, method B: 0.84). This is probably due to the convexity of growth curve ($d \log L / d \log t < 1$) which caused the measurement error in size to be larger than the measurement error in time, and the smallness of interspecies variation in the proportionality constant compared to the measurement error in size. The dashed diagonal line in (C - F) indicates a perfect match between prediction and observation. All error bars are the standard errors calculated by the law of propagation of uncertainty.

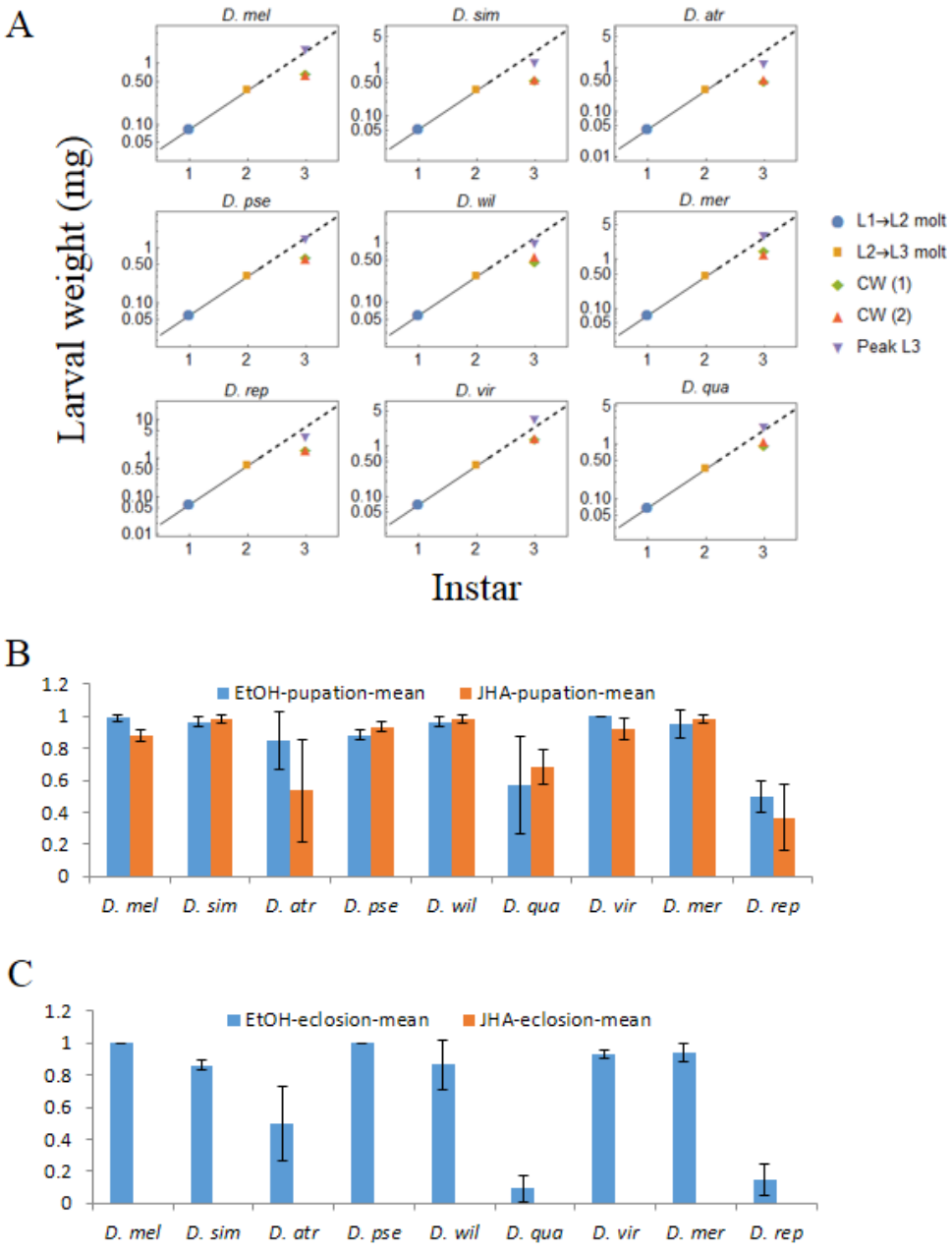

Figure S5. Differences in pupal commitment mechanisms between *Drosophila* and *Manduca*, related to Figure 4.

(A) Relationship between size at molting and critical weight (Dyar's rule). In *Manduca*, critical weight can be predicted by extrapolating the log-linear relation of larval size at molting between each instar (Dyar's rule). However, values predicted in this way were significantly larger than the experimentally observed critical weight of the nine *Drosophila* species in this study. Rather, the peak size of feeding larvae was consistent with this relationship. **(B and C)** Effects of juvenile hormone on pupation rate and eclosion rate. Comparison of (B) pupation rate and (C) eclosion rate between the EtOH-treated

group and JHA-treated group in each species. Each bar indicates mean ± SD of triplicates of 20-30 animals. There was no significant difference in pupation rate between the two groups ($p = 0.21$, two-way ANOVA), whereas the eclosion rate was significantly different between the two groups ($p < 0.01$, two-way ANOVA). We did not observe an eclosed adult in the JHA-applied group for any species.

Supplementary table

Table S1. Data of *Manduca sexta*, related to Figure 4.

	Predicted ($c = 0.24, k = 0.94$)	Observed (Minimum viable weight)	Observed (Critical weight)
Relative size	0.21	0.29	0.63
Relative timing	0.91	0.86	0.92

Transparent Methods

Fly stocks and rearing

In this study, Oregon R (*OreR*) strain was used as wild-type for *D. melanogaster*, and other species (*D. simulans, D. atripex, D. willistoni, D. pseudoobscura, D. quadrilineata, D. virilis, D. mercatorum,* and *D. repleta*) were derived from strains maintained in EHIME-fly, a laboratory for *Drosophila* resources at Ehime University. All flies were reared at 25°C on standard food containing 8 g of agar, 100 g of glucose, 45 g of dry yeast, 40 g of corn flour, 4 ml of propionic acid, 0.45 g of butylparaben (in ethanol) per liter.

Measurement of growth curves

After a 2-4 h egg-laying period, eggs were transferred onto the food to maintain a density of 20-40 individuals per vial. Then, after a defined feeding period, flies of mixed sexes were weighed in more than three batches of about 10 individuals (or 50 individuals for 1st instar larvae) for each time-point. Larvae and pupae were washed with phosphate-buffered saline and carefully dried with a Kimwipe before weighing. Adults were weighed after being anaesthetized with carbon dioxide. We calculated “time after hatching” (x-axis of growth curve) by subtracting "average hatching times" from "time after egg laying" (hatching time was measured by time-lapse imaging of eggs with a digital camera). Timing of “cessation of growth” was defined as the point when weight no longer increased by 10% or more since the previous time-point. For the growth curve of the imaginal disc in **Figure 5B**, the wing disc was giemsa-stained, photographed with a Zeiss Primo Star microscope equipped with a AxioCam ERc 5s digital camera (Zeiss), and its area was measured by Image J.

Starvation experiments

For each species, the mixed-sex third instar larvae of various sizes were removed from the food source and photographed under a stereomicroscope (Zeiss) with a digital camera (Canon) to quantify their size. We determined the volume of the larvae using the prolate spheroid formula $4/3\pi(L/2)(l/2)^2$ (where L is the length and l is the width). Note that the volume (mm^3) and mass (mg) can be converted to each other by using water density ($1\ \mathrm{mg/mm}^3$), as shown in Figure S1A. Then, each measured sample was transferred to one well of a 48-well plate filled with 0.8% agar medium to prevent dehydration. The agar plate on which larvae were transferred was placed in a 25°C incubator and photographed every hour with a Canon EOS Kiss X7 digital camera (Canon). After 10 days, we checked whether each larva became a pupa or not (data for method 1). If it became a pupa, we recorded the time taken to pupariate from the time-lapse images (data for method 2).

Calculating critical size

From the starvation experiment, we calculated critical size using two alternative statistical methods (method A, based on pupariation rate; or method B, based on pupariation time). Method A addresses whether the larvae became pupae or not, as a binary function of larval size (0 = not pupariated, 1 = pupariated) and uses logistic regression to detect "a size that entails 50% probability of becoming a pupa," which is regarded as a critical size (De Moed et al., 1999; Mirth et al., 2005; Ohhara et al., 2017). Method B addresses the time to pupariation as a function of larval size and uses segmented linear regression (SLR) to detect a breakpoint, wherein the x-value is regarded as a critical size (Callier et al., 2013; Ghosh et al., 2013; Stieper et al., 2008; Testa et al., 2013). Because it is technically difficult for a conventional SLR method to detect breakpoints close to the end points of data, we developed a SLR method that can robustly detect breakpoints (SI Text S3). For both methods A and B, we calculated the average and standard deviation of critical size from 1000 bootstrapped samples of each species.

Calculating molting size

For each species, mixed-sex larvae of various instar stages were taken from the food source and their volume was measured in the same manner described above. We determined larval stages by observing spiracle and mouth hook morphology (Ashburner et al., 2005). We treated whether the larva were the (n)th instar or the (n+1)th instar as a binary function of larval size [(n)th = 0, (n+1)th = 1], and used logistic regression to detect "size at the time when there was a 50% mix of (n)th and (n+1n)th larvae " which is regarded as the molting size of (n)th instar (n = 1, 2).

Application of JHA

For each species, the feeding third instar larvae of mixed sexes were taken from the food source, divided into two groups of the same size (20-30 animals), and each group was transferred to a new food source. On a new food source, 30 μl of the JH analog methoprene (SIGMA, diluted to 10 ppm with ethanol) was topically applied to one group, and the same amount of ethanol was applied as a control to the other group. For each group, we measured the rate of pupation and eclosion. Experiments were repeated three times and statistical tests were performed by two-way repeated ANOVA.

Quantification of ecdysteroids by LC-MS/MS

Quantification of ecdysteroids was performed as previously described (Lavrynenko et al., 2015) with some modifications. Frozen samples in 1.5 ml plastic tubes were homogenized in 200 μl cold methanol containing 100 pg muristerone A (MuA, internal standard) with 1x ϕ 3 mm zirconia beads using a freeze crusher (Tokken Inc.). The homogenates were mixed with 100 μl of methanol, 100 μl of H_2O, and 100 μl of $CHCl_3$, and vortexed for 20 min at RT. The samples were centrifuged at 15,000 rpm (20,000 *g*) for 15 min at 4°C. The pellets were washed with 300 μl ethanol, re-dissolved with 300

µl of 0.2 N NaOH, and used to quantify protein using a BCA protein assay kit (Thermo). The supernatant was mixed with 200 µl of H_2O and vortexed for 10 min at RT. The samples were centrifuged at 15,000 rpm for 15 min at 4°C, and the aqueous phase was collected and dried down in a vacuum concentrator. The dried material was re-dissolved in 300 µl of 20% methanol. The samples were loaded on MonoSpin C18 columns (GL Sciences Inc.). The columns were pre-washed with 200 µl methanol and water. Upon sample loading and centrifuged for 1 min at 4,000 *g*, columns were washed with 300 µl 20% methanol. The samples were eluted with 300 µl of 60% methanol. The eluates were dried down, re-dissolved in 10% methanol, and analyzed by Liquid Chromatography with tandem Mass Spectrometry (LC-MS/MS).

Chromatographic separation was performed on an ACQUITY BEH C18 column (50 mm x 2.1 mm, 1.7-µm particles, Waters) in combination with a VanGuard precolumn (5 mm x 2.1 mm, 1.7-µm particles) using an Acquity UPLC H-Class System (Waters). The mobile phase delivered at a flow rate of 0.25 ml/min at 40°C, consisting of solvent A: 0.1% formic acid in acetonitrile, and solvent B: 0.1% formic acid in H_2O. Linear gradients were as follows: 15% A at 0-0.5 min, 15-40% A at 0.5-2 min, 40% at 2-2.5 min, and 15% at 2.5-5 min. The mass spectrometric analysis was performed using a Xevo TQD triple quadrupole mass spectrometer (Waters) coupled with an electro-spray ionization source in the positive ion mode. The MRM transitions were as follows: 20E, *m/z* 481.2 -> 165.2 and 371.3; MuA, *m/z* 497.3 -> 297.2 and 425.3. We optimized analytical conditions using standards solution of 20E (Sigma) and MuA (AG Scientific). Sample concentrations were calculated from a standard curve obtained from serial dilution of each standard, and then normalized to an internal standard and protein values.

Derivation of optimal scaling relationship

For the feeding larval stage ($t \in [0, t_{CG}]$), the growth dynamics of larval and imaginal tissue sizes (L and I, respectively) obey the following equation (Figure 2A):

$$\frac{dL}{dt} = u(t)E(L) \qquad \text{[S1A]}$$

$$\frac{dI}{dt} = \big(1 - u(t)\big)E(L), \qquad \text{[S1B]}$$

where $E(L) \coloneqq gL^k$ is the total amount of energy (available for growth) obtained from the environment by larval feeding. The parameters g and k are the assimilation rate coefficient and growth scaling exponent, respectively (Bonduriansky and Day, 2003; Day and Taylor, 1997; Hou et al., 2008). The acquired energy is allocated to the growth of larval and imaginal tissue according to a

ratio of $u:1-u$ under a constraint ($b_L \leq u \leq 1-b_I$, assuming that fixed ratio of energy b_L and b_I are always allocated to the larval and imaginal tissue, respectively).

For the non-feeding larval/pupal stage ($t \in [t_{CG}, t_{EC}]$), the size of larval and imaginal tissues at the cessation of net growth (L_{CG} and I_{CG}, respectively) is summed up to the adult body size A_{EC} (Figure 2B):

$$A_{EC} = cL_{CG} + I_{CG}, \qquad \text{[S2]}$$

where c $(0 < c < 1)$ is the efficiency of energy reallocation.

The growth schedule, which is governed by the energy allocation time course $u(t)$, is optimized for the entire larval period, based on the idea that the life history appears as a result of adaptive evolution (Roff, 2002). The fitness maximized here is assumed to be an increasing function of the adult size: $\phi = \phi(A_{EC}), d\phi/dA_{EC} > 0$ (for more general fitness, please see (Hironaka and Morishita, 2017)). Using Pontryagin's maximum principle, we can find that the optimal energy allocation u^* is biphasic. This is the so-called "bang-bang" control, which is the common solution for linear control systems (Kirk, 2012). Namely, u^* takes the upper limit value $1-b_I$ until a certain switching time t_{CS}, and thereafter takes the lower limit value b_L:

$$u^*(t) = \begin{cases} 1-b_I & 0 < t < t_{CS} \\ b_L & t_{CS} < t < t_{CG} \end{cases} \qquad \text{[S3]}$$

Furthermore, Pontryagin's maximum principle can also instantly lead to the optimal scaling relationship of critical size (Hironaka and Morishita, 2017). Alternatively, assuming the bang-bang control (Eq. S3), we can derive the optimal scaling by standard differential calculus. Hereafter we describe the latter procedure. First, substituting Eq. S3 into Eqs. S1, the growth curve of each tissue can be written as follows:

$$L(t) = \begin{cases} \left[L_0^{1-k} + g(1-k)(1-b_I)t\right]^{\frac{1}{1-k}} & 0 < t < t_{CS} \\ \left[L_{CS}^{1-k} + g(1-k)b_L t\right]^{\frac{1}{1-k}} & t_{CS} < t < t_{CG} \end{cases} \qquad \text{[S4A]}$$

$$I(t) = \begin{cases} I_0 + \dfrac{b_I}{1-b_I}(L(t) - L_0) & 0 < t < t_{CS} \\ I_{CS} + \dfrac{1-b_L}{b_L}(L(t) - L_{CS}) & t_{CS} < t < t_{CG} \end{cases} \qquad \text{[S4B]}$$

where L_0 and I_0 are parameters describing initial size of larval and imaginal tissue, respectively. We also introduced the notation $L_{CS} \coloneqq L(t_{CS})$ and $I_{CS} \coloneqq L(t_{CS})$ to denote the size of larval and imaginal tissue at critical time, respectively. Now let us remind that the fitness to be maximized can be written as follows:

$$\phi = \phi(A_{EC}) = \phi(L_{CG}, I_{CG}) \qquad \text{[S5]}$$

where $L_{CG} \coloneqq L(t_{CG})$ and $I_{CG} \coloneqq L(t_{CG})$. Note that both L_{CG} and I_{CG} can be regarded as functions of the switching time t_{CS}: $L_{CG} = L_{CG}(t_{CS})$, $I_{CG} = I_{CG}(t_{CS})$. Thus, in order for t_{CS} to optimize ϕ, the following condition must be satisfied:

$$\frac{d\phi}{dt_{CS}} = \frac{\partial\phi}{\partial L_{CG}}\frac{dL_{CG}}{dt_{CS}} + \frac{\partial\phi}{\partial I_{CG}}\frac{dI_{CG}}{dt_{CS}} = 0 \qquad \text{[S6]}$$

Solving this equation using Eqs. S4, we obtain the scaling relationship between the critical size and the final larval size:

$$\frac{L_{CS}}{L_{CG}} = \left[1 - b_L\left(1 - \frac{\partial_L\phi}{\partial_I\phi}\right)\right]^{\frac{1}{k}} \qquad \text{[S7]}$$

where $\partial_L\phi \coloneqq \partial\phi/\partial L_{CG}$ and $\partial_I\phi \coloneqq \partial\phi/\partial I_{CG}$. Moreover, assuming that larval tissue size immediately after hatching is negligible $(L_0 \approx 0)$, the above equation leads to the equation that describes the scaling relationship between the critical time and the total development time:

$$\frac{t_{CS}}{t_{CG}} \approx \frac{b_L}{b_L + (1 - b_I)\left\{\left[1 - b_L\left(1 - \frac{\partial_L\phi}{\partial_I\phi}\right)\right]^{\frac{k-1}{k}} - 1\right\}} \qquad \text{[S8]}$$

Because Eqs. S7 and S8 have the fitness function ϕ on the right hand side, the scaling coefficients are not necessarily be constant, but are dependent on the final size or development time through the functional form of ϕ. However, in the case of holometabolous insects, due to the assumption of energy reallocation $\phi = \phi(cL_{CG} + I_{CG})$ (Eqs. S2 and S5), we can use the following relationship:

$$\frac{\partial_L \phi}{\partial_I \phi} = \frac{\partial_L A_{EC}}{\partial_I A_{EC}} = c \qquad \text{[S9]}$$

Substituting this into Eqs. S7 and S8, we obtain:

$$\frac{L_{CS}}{L_{CG}} = [1 - b_L(1-c)]^{\frac{1}{k}} \qquad \text{[S7']}$$

$$\frac{t_{CS}}{t_{CG}} \approx \frac{b_L}{b_L + (1-b_I)\left\{[1 - b_L(1-c)]^{\frac{k-1}{k}} - 1\right\}} \qquad \text{[S8']}$$

Eventually, the scaling pattern (e.g., linear or nonlinear) depends only on four growth parameters, which appear on the right hand side of these equations: $b_I, b_L, c,$ and k. If these four parameters are constant between species, the scaling pattern is linear and the final size is proportional to the critical size. At this time, by assuming the exponential growth during the TGP (Nijhout et al., 2006; Shingleton et al., 2008; Vollmer et al., 2016), an inversely proportional relationship between the TGP and growth rate emerges:

$$\begin{cases} [\text{Final size}] \propto [\text{Critical size}] \\ [\text{Final size}] = [\text{Critical size}] * \exp([\text{Growth rate}] * [\text{TGP}]) \end{cases}$$

$$\Rightarrow \log \frac{[\text{Final size}]}{[\text{Critical size}]} = [\text{Growth rate}] * [\text{TGP}] = \text{const.}$$

$$\Rightarrow [\text{Growth rate}] \propto [\text{TGP}]^{-1}$$

Estimation of growth parameters from experimentally measurable quantities

How can we estimate values of the growth parameters b_I, b_L, c and k in real organisms? Regarding b_I and b_L, we can use the following relationships derived from Eq. S4B:

$$b_I = \frac{\Delta I_{PRE}}{\Delta L_{PRE} + \Delta I_{PRE}} \qquad \text{[S10A]}$$

$$b_L = \frac{\Delta L_{TGP}}{\Delta L_{TGP} + \Delta I_{TGP}} \qquad \text{[S10B]}$$

where $\Delta X_{TGP} \coloneqq X_{CG} - X_{CS}$ and $\Delta X_{PRE} \coloneqq X_{CS} - X_0$ indicates the amount of growth in variable X (L or I) before and after the critical size attainment, respectively. Because imaginal tissues are negligible compared to larval tissues during the whole larval stage, we can assume $L(t) \gg$

$I(t)$ for $0 \leq t \leq t_{CG}$, and therefore we can expect that $b_L \approx 1$ and $b_I \approx 0$ hold true in real organisms. This means that the ratio of controllable energy is small and most energy is allocated to the larval tissues (see Figure 2 and Eq. S1). Applying this assumption to Eqs. S7' and S8', we obtain the simplified form of scaling relationships:

$$L_{CS} \approx c^{\frac{1}{k}} L_{CG} \quad \text{[S7"]}$$

$$t_{CS} \approx c^{\frac{1-k}{k}} t_{CG} \quad \text{[S8"]}$$

Interestingly, these equations indicate that, even in an extreme case where the controllable energy is very small, both the optimal critical size and optimal critical time do not take a limit value such as L_{CG} and t_{CG}, but rather take an intermediate value.

Under the above assumptions ($L_0 \approx 0, b_L \approx 1, b_I \approx 0$ and $L_{CG} \gg I_{CG}$), the remaining two parameters c and k can be estimated by using Eq. S2 and Eq. S4A (i.e., $L(t) \approx [g(1-k)t]^{\frac{1}{1-k}}$), respectively:

$$c \approx \frac{A_{EC}}{L_{CG}} \quad \text{[S11A]}$$

$$k \approx 1 - \left(\frac{d \log L}{d \log t}\right)^{-1} \quad \text{[S11B]}$$

where $d \log L / d \log t$ is the slope in the double logarithmic plot of the growth curve from hatching until growth cessation. Therefore, the value of c can be obtained from Figure 3B and the value of k can be obtained by fitting the growth curve with a power function $y = ax^b$ and then converting by $k = 1 - 1/b$ (Figure S1D).

The constancy of c between two species means that the % weight loss during the non-feeding period (i.e., the wandering larval and pupal period) is the same for those species. In contrast, the constancy of k between two species means that the two larval growth curves perfectly overlap if normalized by the final size and the total development time.

Rotation-free segmented linear regression

In a conventional segmented linear regression (SLR) (Muggeo, 2008), it is difficult to detect the breakpoint close to the end points of data for the x-coordinates. These type of data are often observed in a relationship between the larval size and the time to pupariation in *Drosophila* (Callier et al., 2013; Ghosh et al., 2013; Testa et al., 2013). The difficulty in obtaining the correct regression line is likely

due to error amplification caused by the steep slope (Figure S4A, left panel). In previous studies, as a practical approach to solve this problem, the whole data is rotated 0.5 degrees around the origin before regression (Callier et al., 2013; Ghosh et al., 2013; Testa et al., 2013). However, in this rotation-based SLR method, the rotation angle is arbitrary and must be determined optimally depending on the characteristics of existing data (such as the ratio of the data range of x to that of y). To avoid these difficulties, we developed a rotation-free SLR method that can detect a breakpoint independently of data characteristics. Because our method accounts for errors not only in y-axis (dependent variables), but also in x-axis (independent variables), error amplification does not occur no matter how steep the true slope is. Furthermore, to make the regression invariant to the scale of variables (i.e., dimension or unit), the residuals, which are defined by perpendicular distances to the regression line from the data points, are calculated after data standardization (Figure S4A, right panel). We describe the detailed procedure in the following five steps:

---

1. Convert data (X_i, Y_i) $(i = 1,2,\cdots n)$ to standardized data (x_i, y_i) according to the following formula:

$$x_i \coloneqq \frac{X_i - \mu_X}{\sigma_X}, y_i \coloneqq \frac{Y_i - \mu_Y}{\sigma_Y}$$

$$\mu_X \coloneqq \frac{1}{n}\sum_{i=1}^{n} X_i\,, \mu_Y \coloneqq \frac{1}{n}\sum_{i=1}^{n} Y_i\,, \sigma_X^2 \coloneqq \frac{1}{n}\sum_{i=1}^{n}(X_i - \mu_X)^2\,, \sigma_Y^2 \coloneqq \frac{1}{n}\sum_{i=1}^{n}(Y_i - \mu_Y)^2$$

2. In a standardized space, define a segmented linear regression equation with two segments:

$$y = \begin{cases} a_1(x - x_0) + y_0 & x \le x_0 \\ a_2(x - x_0) + y_0 & x > x_0 \end{cases}$$

3. For this regression line, define the residual sum of squares E based on the shortest distance d from each data point (i.e., the shorter one of the two perpendiculars):

$$E(a_1, a_2, x_0, y_0) \coloneqq \sum_{i=1}^{n} d(x_i, y_i | a_1, a_2, x_0, y_0)^2$$

$$d(x_i, y_i | a_1, a_2, x_0, y_0) \coloneqq \min\left\{\frac{|(y_i - y_0) - a_1(x_i - x_0)|}{\sqrt{1 + a_1^2}}, \frac{|(y_i - y_0) - a_2(x_i - x_0)|}{\sqrt{1 + a_2^2}}\right\}$$

4. Obtain a regression line that minimizes the residual sum of squares by the simulated annealing:

4-1. Search the new point candidate $\{a_1', a_2', x_0', y_0'\}$ by perturbing the current point $\{a_1, a_2, x_0, y_0\}$. Note that candidate points cannot be efficiently sampled unless a probability distribution in angular space is given for variations in the slopes of the straight line, a_1, a_2.

4-2. Calculate the difference of the residual sum of squares, $\Delta E \coloneqq E(a_1', a_2', x_0', y_0') - E(a_1, a_2, x_0, y_0)$.

4-3. If $\Delta E < 0$, adopt the candidate with probability 1; if $\Delta E \geq 0$, adopt with probability $e^{-\beta \Delta E}$. β is an inverse temperature parameter and takes an annealing schedule of $\beta = (1 - T/T_{\max})^{-1}$, where T and $T_{\max}$ are the current and maximum time steps, respectively, where T is initially set as 0.

4-4. Increase T by 1. If $T < T_{\max}$, return to 4-1. If $T = T_{\max}$, end the procedure and go to the next step.

5. Return the regression line to the original scale according to the following equation:

$$Y = \begin{cases} \mu_Y + \sigma_Y \left[a_1 \left(\dfrac{X - \mu_X}{\sigma_X} - x_0 \right) + y_0 \right] & X \leq \mu_X + \sigma_X x_0 \\ \mu_Y + \sigma_Y \left[a_2 \left(\dfrac{X - \mu_X}{\sigma_X} - x_0 \right) + y_0 \right] & X > \mu_X + \sigma_X x_0 \end{cases}$$

Here, the x-coordinates of the breakpoint, $\mu_X + \sigma_X x_0$, corresponds to the critical size.

To test the validity of the proposed method using the published data from the previous study on critical size (Koyama et al., 2014), we compared the breakpoint obtained by the rotation-based SLR with that obtained by our rotation-free SLR. As shown in Figure S5B, a strong correlation ($r = 0.98$) was observed between the two methods, confirming that our method is accurate.

Differences between *Drosophila* and *Manduca*

In the nine *Drosophila* species in this study, we found no large difference in the estimated threshold size values between methods A and B (Figure S3). However, in *Manduca sexta*, the value estimated by method A was usually much smaller than that of method B (Nijhout, 1975; NIJHOUT and WILLIAMS, 1974). The former is called the minimum viable weight (MVW), which can be clearly distinguished from the latter, the critical weight (CW) (Callier and Nijhout, 2013). Interestingly, when we calculate the switching point of optimal energy allocation for *Manduca* based on published literature, its value is much closer to the MVW than the CW (Hironaka and Morishita, 2017) [Table S1]. Additionally, consistent with the expectation from the optimal energy allocation model that imaginal discs begin to grow rapidly after the energy allocation switch (Figure 1B), initiation of *Manduca* imaginal disc growth (observed at 1-2 days of final instar) is slightly earlier than the attainment of the CW (usually occurs at 2-3 days of final instar) (Nijhout et al., 2006; Truman et al.,

2006). These two facts suggest that the energy allocation switch in *Manduca* occurs at the MVW rather than the CW.

In *Manduca*, it is reported that the CW can be predicted by extrapolating the log-linear relationship between larval size at each instar molt (called "Dyar's rule") (Nijhout et al., 2006). Namely, the predicted weight at a presumptive fifth to sixth instar molt is very close to the CW (note that the fifth instar is usually the final instar for *Manduca*). However, in these nine *Drosophila* species, this method of weight estimation fails to predict the CW and has an obviously larger value than the CW (Figure S5A). These observations also imply that the CW of *Manduca* refers to a physiologically different checkpoint than the CW of *Drosophila*.

A previous study suggested that the different CW behavior between *Manduca* and *Drosophila* is derived from a different JH effect in metamorphosis (Hatem et al., 2015). Consistent with this idea, topical JH application did not suppress pupation of nine *Drosophila* species, unlike *Manduca*, although the eclosion of pupae was completely suppressed for all species (Figure S5B).

References

Ashburner, M., Golic, K.G., Hawley, R.S., 2005. Drosophila : a laboratory handbook. Cold Spring Harbor Laboratory Press.

Bonduriansky, R., Day, T., 2003. THE EVOLUTION OF STATIC ALLOMETRY IN SEXUALLY SELECTED TRAITS. Evolution (N. Y). 57, 2450–2458. doi:10.1111/j.0014-3820.2003.tb01490.x

Callier, V., Nijhout, H., 2013. Body size determination in insects: a review and synthesis of size-and brain-dependent and independent mechanisms. Biol. Rev.

Callier, V., Shingleton, A.W., Brent, C.S., Ghosh, S.M., Kim, J., Harrison, J.F., 2013. The role of reduced oxygen in the developmental physiology of growth and metamorphosis initiation in Drosophila melanogaster. J. Exp. Biol. 216, 4334–40. doi:10.1242/jeb.093120

Day, T., Taylor, P.D., 1997. Von Bertalanffy's Growth Equation Should Not Be Used to Model Age and Size at Maturity. Am. Nat. 149, 381–393.

De Moed, G.H., Kruitwagen, C.L.J.J., De Jong, G., Scharloo, W., 1999. Critical weight for the induction of pupariation in Drosophila melanogaster: genetic and environmental variation. J. Evol. Biol. 12, 852–858. doi:10.1046/j.1420-9101.1999.00103.x

Ghosh, S.M., Testa, N.D., Shingleton, A.W., 2013. Temperature-size rule is mediated by thermal plasticity of critical size in Drosophila melanogaster. Proc. Biol. Sci. 280, 20130174. doi:10.1098/rspb.2013.0174

Hatem, N.E., Wang, Z., Nave, K.B., Koyama, T., Suzuki, Y., 2015. The role of juvenile hormone and insulin/TOR signaling in the growth of Manduca sexta. BMC Biol. 13, 44. doi:10.1186/s12915-015-0155-z

Hironaka, K., Morishita, Y., 2017. Adaptive significance of critical weight for metamorphosis in holometabolous insects. J. Theor. Biol. doi:10.1016/j.jtbi.2017.01.014

Hou, C., Zuo, W., Moses, M.E., Woodruff, W.H., Brown, J.H., West, G.B., 2008. Energy uptake and allocation during ontogeny. Science 322, 736–9. doi:10.1126/science.1162302

Kirk, D.E., 2012. Optimal Control Theory: An Introduction. Dover Publications, New York.

Koyama, T., Rodrigues, M.A., Athanasiadis, A., Shingleton, A.W., Mirth, C.K., 2014. Nutritional control of body size through FoxO-Ultraspiracle mediated ecdysone biosynthesis. Elife 3, e03091. doi:10.7554/eLife.03091

Lavrynenko, O., Rodenfels, J., Carvalho, M., Dye, N.A., Lafont, R., Eaton, S., Shevchenko, A., 2015. The Ecdysteroidome of Drosophila: influence of diet and development. Development 142, 3758–68. doi:10.1242/dev.124982

Mirth, C., Truman, J.W., Riddiford, L.M., 2005. The role of the prothoracic gland in determining critical weight for metamorphosis in Drosophila melanogaster. Curr. Biol. 15, 1796–807. doi:10.1016/j.cub.2005.09.017

Muggeo, V.M.R., 2008. Segmented: an R package to fit regression models with broken-line relationships. R news 8, 20–25.

Nijhout, H., 1975. A threshold size for metamorphosis in the tobacco hornworm, Manduca sexta (L.). Biol. Bull.

Nijhout, H.F., Davidowitz, G., Roff, D.A., 2006. A quantitative analysis of the mechanism that controls body size in Manduca sexta. J. Biol. 5, 16. doi:10.1186/jbiol43

NIJHOUT, H.F., WILLIAMS, C.M., 1974. Control of Moulting and Metamorphosis in the Tobacco Hornworm, Manduca Sexta (L.): Growth of the Last-Instar Larva and the Decision to Pupate. J. Exp. Biol. 61.

Ohhara, Y., Kobayashi, S., Yamanaka, N., Kaynig, V., Longair, M., Pietzsch, T., 2017. Nutrient-Dependent Endocycling in Steroidogenic Tissue Dictates Timing of Metamorphosis in Drosophila melanogaster. PLOS Genet. 13, e1006583. doi:10.1371/journal.pgen.1006583

Roff, D., 2002. Life history evolution. Sinauer Associates, Massachusetts.

Shingleton, A.W., Mirth, C.K., Bates, P.W., 2008. Developmental model of static allometry in holometabolous insects. Proc. Biol. Sci. 275, 1875–85. doi:10.1098/rspb.2008.0227

Stieper, B.C., Kupershtok, M., Driscoll, M. V, Shingleton, A.W., 2008. Imaginal discs regulate developmental timing in Drosophila melanogaster. Dev. Biol. 321, 18–26. doi:10.1016/j.ydbio.2008.05.556

Testa, N.D., Ghosh, S.M., Shingleton, A.W., 2013. Sex-specific weight loss mediates sexual size dimorphism in Drosophila melanogaster. PLoS One 8, e58936. doi:10.1371/journal.pone.0058936

Truman, J.W., Hiruma, K., Allee, J.P., Macwhinnie, S.G.B., Champlin, D.T., Riddiford, L.M., 2006. Juvenile hormone is required to couple imaginal disc formation with nutrition in insects. Science 312, 1385–8. doi:10.1126/science.1123652

Vollmer, J., Iber, D., Ahuja, C., Eswaran, H., Nijhout, H.F., 2016. An Unbiased Analysis of Candidate Mechanisms for the Regulation of Drosophila Wing Disc Growth. Sci. Rep. 6, 39228. doi:10.1038/srep39228